Activation of 5-HT2A receptors upregulates the function of the neuronal K-Cl cotransporter KCC2

Rémi Bos, K. Sadlaoud, P. Boulenguez, D. Buttigieg, Sophie Liabeuf, C. Brocard, G. Haase, H. Bras, L. Vinay

Activation of 5-HT2A receptors upregulates the function of the neuronal K-Cl cotransporter KCC2

Rémi Bos, Karina Sadlaoud, Pascale Boulenguez, Dorothée Buttigieg, Sylvie Liabeuf, Cécile Brocard, Georg Haase, Hélène Bras, and Laurent Vinay[1]

Institut de Neurosciences de la Timone, Unité Mixte de Recherche 7289, Centre National de la Recherche Scientifique, Aix-Marseille Université, F-13385 cx5 Marseille, France

Edited by Sten Grillner, Karolinska Institutet, Stockholm, Sweden, and approved November 15, 2012 (received for review August 8, 2012)

In healthy adults, activation of γ-aminobutyric acid $(GABA)_A$ and glycine receptors inhibits neurons as a result of low intracellular chloride concentration ($[Cl^-]_i$), which is maintained by the potassium-chloride cotransporter KCC2. A reduction of KCC2 expression or function is implicated in the pathogenesis of several neurological disorders, including spasticity and chronic pain following spinal cord injury (SCI). Given the critical role of KCC2 in regulating the strength and robustness of inhibition, identifying tools that may increase KCC2 function and, hence, restore endogenous inhibition in pathological conditions is of particular importance. We show that activation of 5-hydroxytryptamine (5-HT) type 2A receptors to serotonin hyperpolarizes the reversal potential of inhibitory postsynaptic potentials (IPSPs), E_{IPSP}, in spinal motoneurons, increases the cell membrane expression of KCC2 and both restores endogenous inhibition and reduces spasticity after SCI in rats. Up-regulation of KCC2 function by targeting $5\text{-}HT_{2A}$ receptors, therefore, has therapeutic potential in the treatment of neurological disorders involving altered chloride homeostasis. However, these receptors have been implicated in several psychiatric disorders, and their effects on pain processing are controversial, highlighting the need to further investigate the potential systemic effects of specific $5\text{-}HT_{2A}$R agonists, such as (4-bromo-3,6-dimethoxybenzocyclobuten-1-yl)methylamine hydrobromide (TCB-2).

The neuron-specific K^+-Cl^- cotransporter KCC2 (encoded by the solute carrier family 12 member 5, *Slc12a5*) extrudes Cl^- and is responsible for the low $[Cl^-]_i$ in mature neurons (1–3), a prerequisite for hyperpolarizing inhibition mediated by $GABA_A$ receptors ($GABA_A$Rs) and glycine receptors (GlyRs). The expression or the function of KCC2 is reduced in several neurological disorders (2, 4), and the resulting slight increase in $[Cl^-]_i$ (depolarizing shift of the chloride equilibrium potential, E_{Cl}) dramatically compromises the inhibitory control of firing rate and excitatory inputs (5–7). Given the role of KCC2 in regulating the strength of inhibitory synaptic transmission, identifying tools that may increase KCC2 function and, hence, restore endogenous inhibition in pathological conditions is of particular importance.

Spasticity is a disabling complication affecting individuals with spinal cord injury (SCI) and is characterized by a velocity-dependent increase in muscle tone resulting from hyperexcitable stretch reflexes, spasms, and hypersensitivity to normally innocuous sensory stimulations (8, 9). Down-regulation of KCC2 after SCI in rats is implicated in the development of spasticity (10) and chronic pain (11, 12). Notably, the expression of KCC2 in the motoneuron membrane is reduced, and, concomitantly, the density of cytoplasmic clusters is higher, suggesting that the surface stability of the transporter is reduced in these pathological conditions (10).

Mounting evidence indicates that phosphorylation of KCC2 in the C-terminal intracellular domain dynamically regulates its activity and surface expression (1). In particular, phosphorylation by protein kinase (PK)C, enhances KCC2 activity and reduces endocytosis (13). Interestingly, activation of 5-hydroxytryptamine type 2 receptors ($5\text{-}HT_2$Rs) to serotonin stimulates PKC and strengthens the left–right alternation of motor bursts observed during locomotion (14–16), which rely on reciprocal inhibition (17, 18). We hypothesized that $5\text{-}HT_2$R activity modulates KCC2 function and/or expression. Our results indicate that the activation of the $5\text{-}HT_{2A}$R subtype hyperpolarizes E_{IPSP} via a PKC-dependent mechanism, increases KCC2 expression in the plasma membrane of motoneurons, and reduces SCI-induced spasticity.

Results

Negative Shift of E_{IPSP} and Up-Regulation of KCC2. We first examined the effect of the $5\text{-}HT_{2A/2B/2C}$R agonist (±)-2,5-dimethoxy-4-iodoamphetamine hydrochloride (DOI) (10 μM; Table S1) on E_{IPSP} in control neonatal rats [postnatal day (P)5–P7]. DOI-hyperpolarized E_{IPSP} within 10–20 min (Fig. 1 *A* and *B*). This effect was long-lasting (at least 2 h; Fig. 1*B*). E_{IPSP} was significantly more hyperpolarized when motoneurons were recorded in the presence of DOI compared with control (8 mV; Fig. 1*C*, *Left*). There was a concomitant trend toward a depolarization of the resting membrane potential (V_{rest}) by DOI (+2 mV; $P > 0.05$). As a result, the amplitude of hyperpolarizing IPSPs recorded at V_{rest} increased significantly (Fig. 1*C*, *Right*).

The next series of experiments was performed on animals that underwent a neonatal SCI. E_{IPSP} was significantly more depolarized in those animals tested at P5–P7, compared with controls of the same age, as shown previously (19) (compare Fig. 1 *C* and *D*). Because of the increased sensitivity of neurons to 5-HT in those animals (15), DOI was tested at a lower concentration (1–1.5 μM) than in controls. DOI induced an ∼8-mV hyperpolarization of E_{IPSP} (Fig. 1*D*, *Left*). As a result, E_{IPSP} shifted from above to below V_{rest} (Fig. 1*D*, *Right*). Another set of animals was treated chronically with DOI from P4 to P6–P7 [0.15 mg/kg, i.p. (15, 20) twice a day]. E_{IPSP} was more hyperpolarized in those DOI-treated animals than in untreated transected animals (Fig. 1*E*). Values were similar to those measured in control animals.

We performed subcellular fractionation of proteins from the lumbosacral spinal cord, followed by immunoblotting with a specific antibody against KCC2. The amount of KCC2 in the membrane fraction (KCC2Mb) was significantly increased after chronic DOI treatment, compared with NaCl-treated pups (Fig. 1*F*). There was a trend toward an increase in the amount of KCC2 in the cytosolic fraction. As a result, the ratio KCC2Mb/KCC2 cytoplasm was nonsignificantly increased. We then analyzed the expression of KCC2 by immunohistochemistry. All of the analyses were performed on a homogeneous population of retrogradely labeled lumbar motoneurons [triceps surae (TS) muscles (ankle extensors); Fig. 1*G*]. GlyRs are colocalized with the anchoring protein gephyrin and can, therefore, be used to label the plasma

Author contributions: R.B. and L.V. designed research; R.B., K.S., P.B., D.B., S.L., C.B., G.H., H.B., and L.V. performed research; G.H. contributed new reagents/analytic tools; R.B., K.S., P.B., D.B., S.L., C.B., H.B., and L.V. analyzed data; and R.B. and L.V. wrote the paper.

The authors declare no conflict of interest.

This article is a PNAS Direct Submission.

[1]To whom correspondence should be addressed. E-mail: laurent.vinay@univ-amu.fr.

This article contains supporting information online at www.pnas.org/lookup/suppl/doi:10.1073/pnas.1213680110/-/DCSupplemental.

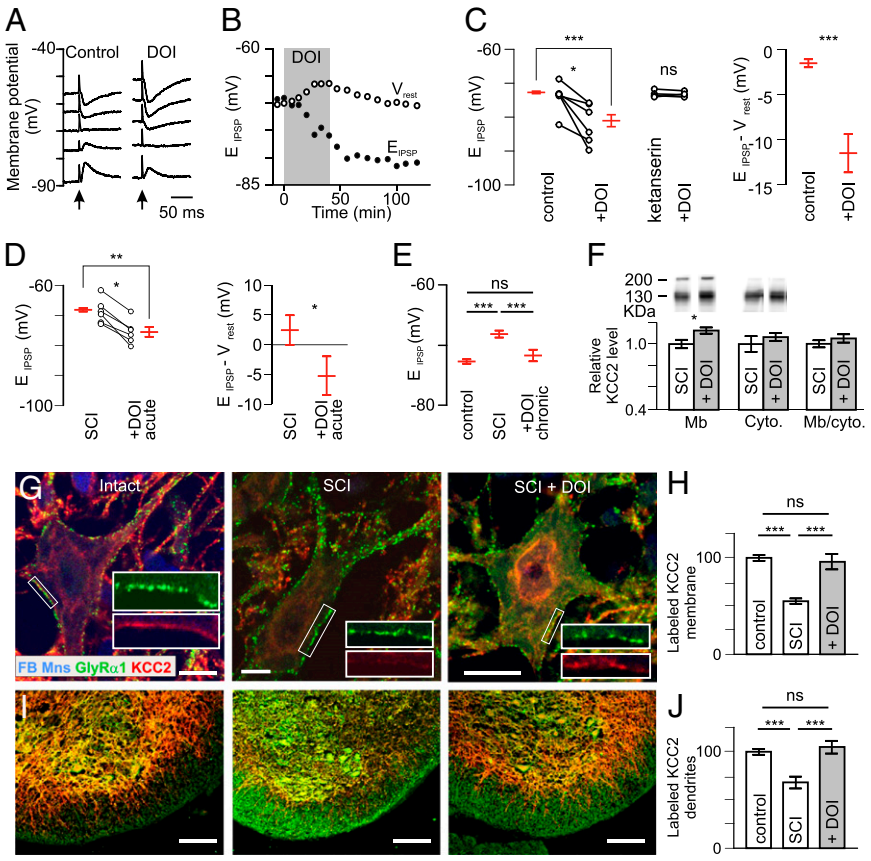

Fig. 1. Activation of 5-HT$_2$Rs hyperpolarizes E_{IPSP} and increases membrane expression of KCC2. (*A*) IPSPs evoked by stimulation of the ventral funiculus of the spinal cord (arrow) at different holding potentials in a motoneuron from a P6 intact rat before and after adding DOI (10 μM). (*B*) Time course of the change in E_{IPSP} and V_{rest}. (*C*) E_{IPSP} and driving force (E_{IPSP}-V_{rest}) measured in control conditions ($n = 21$) and after adding DOI ($n = 8$). ***$P < 0.001$ (Mann–Whitney test). Six motoneurons were tested before and after DOI. *$P < 0.05$ (Wilcoxon paired test). The effects of DOI were prevented in the presence of ketanserin (10 μM; $n = 4$) (*Center*). (*D*) Effects of DOI (1–1.5 μM) on E_{IPSP} and driving force in motoneurons recorded 4–6 d after neonatal SCI (17 and 6 cells recorded in the absence and the presence of DOI, respectively). **$P < 0.01$, *$P < 0.05$ (Mann–Whitney test); *$P < 0.05$ (Wilcoxon paired test). (*E*) E_{IPSP} was significantly more hyperpolarized after chronic treatment of DOI ($n = 9$) compared with SCI animals ($n = 22$) but not different compared with control animals ($n = 21$). ns, not significant ($P > 0.05$); ***$P < 0.001$ (one-way ANOVA, Tukey's post tests). (*F*, *Upper*) Western blots of membrane and cytoplasmic fractions of lumbar spinal cords labeled with a KCC2-specific antibody. The 130- to 140-kDa and the >200-kDa bands correspond to the monomeric and oligomeric proteins, respectively (53). (*F*, *Lower*) Quantification of KCC2 expression in DOI-treated rats after neonatal SCI (percentage of untreated rats). *$P < 0.05$ (Mann–Whitney test; $n = 6$ in each group). (*G*) Dual labeling of GlyRα1 and KCC2 on FB-labeled ankle extensor motoneurons, in three conditions (P7): intact, neonatal SCI, and chronic DOI treatment. (Scale bars: 10 μm.) (*H*) Quantification of the density of membrane KCC2 labeling (ratios of labeled pixel surface per somatic perimeter) in intact rats ($n = 34$ motoneurons) and untreated ($n = 41$) or DOI-treated ($n = 44$) rats with neonatal SCI (three rats in each group). ***$P < 0.001$ (Kruskal–Wallis test, Dunn's post tests). (*I*) Ventral part of the lumbar spinal cord exhibiting KCC2-immunopositive dendrites stretching out through the white matter. (Scale bars: 100 μm.) (*J*) Quantification of the KCC2 labeling in the white matter in intact rats ($n = 34$) and untreated ($n = 41$) or DOI-treated ($n = 44$) rats with neonatal SCI. ***$P < 0.001$ (Kruskal–Wallis test, Dunn's post tests).

membrane; in addition, they are not affected by a neonatal spinal cord transection (20). We, therefore, immunolabeled the α1 subunit of this receptor to visualize the plasma membrane of motoneurons in control (intact), untreated (SCI), and DOI-treated cord-transected animals (SCI + DOI; Fig. 1*G*, *Insets*). After SCI, the intensity of KCC2 staining in the somatic membrane was reduced (Fig. 1*H*). DOI treatment increased KCC2 staining, so that no difference was observed compared with controls of the same age. We also quantified the KCC2 staining at the level of motoneuron dendrites that stretch out of the gray matter into the lateral and ventral funiculi (Fig. 1*I*). Similar to what was observed for the somatic membrane, DOI treatment restored the intensity of staining to values seen in controls (Fig. 1*J*). Altogether, these results indicate that the activation of 5-HT$_2$R is able to restore chloride homeostasis (hyperpolarizing shift of E_{IPSP}) after neonatal SCI. An increased expression of KCC2 in the plasma membrane, at least in part, provides the molecular basis of this restoration.

Contribution of 5-HT$_{2A}$Rs. The effects of DOI on E_{IPSP} were prevented in the presence of the 5-HT$_2$R antagonist ketanserin (10 μM; $n = 4$; Fig. 1*C*, *Center*). Because DOI and ketanserin also bind to 5-HT$_{2B}$Rs and 5-HT$_{2C}$Rs (Table S1), to further identify the subtype of 5-HT$_2$R that are involved, we used (4-bromo-3,6-dimethoxybenzocyclobuten-1-yl)methylamine hydrobromide (TCB-2), a high-affinity 5-HT$_{2A}$R agonist (21, 22) (Table S1). TCB-2 at low concentration (0.1 μM; $n = 6$) hyperpolarized E_{IPSP} by ~4 mV in control rats (Fig. 2*A* and *B*, gray). Note that even values that were highly negative (−78 mV) were further hyperpolarized in the presence of TCB-2. The shift was larger (6.1 mV) at a higher concentration (10 μM; $n = 4$; Fig. 2*B*, black). TCB-2 had no effect on V_{rest} and the other electrical properties investigated (Fig. S1). As a result, the driving force (E_{IPSP}-V_{rest}) was significantly increased (Fig. 2*B*; −5.3 mV). We next tested this compound on motoneurons recorded from animals with neonatal SCI. The hyperpolarizing shift (−4.2 mV) induced by TCB-2 (0.1μM) was similar to that seen in control animals (Fig. 2*C*). On average,

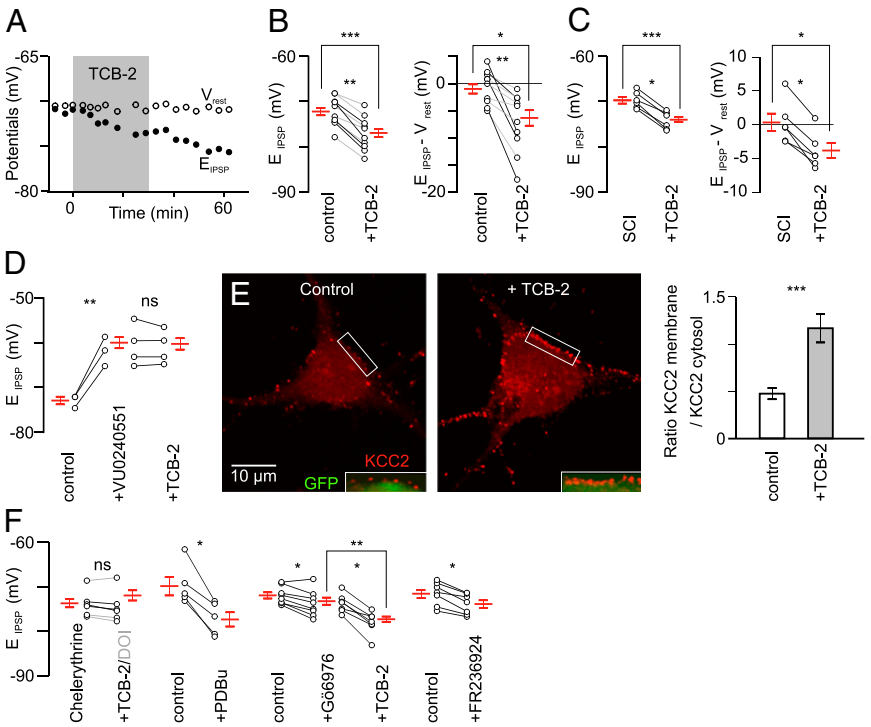

Fig. 2. Involvement of 5-HT$_{2A}$Rs via a PKC-dependent signaling pathway. (*A*) TCB-2 (0.1 μM; 30 min) induces a hyperpolarizing shift of E_{IPSP} without concomitant effect on V_{rest} (P6). (*B*, *Left*) Effect of TCB-2 (0.1 μM, gray; 10 μM, black) on 10 motoneurons recorded from control rats (P5–P6). ***$P < 0.001$ (Mann–Whitney test; $n = 12$ and $n = 14$ before and under TCB-2, respectively); **$P < 0.01$ (Wilcoxon paired test). The difference was also significant when considering only the effect of the lowest concentration [0.1 μM; $n = 6$; *$P < 0.05$ (Wilcoxon paired test)]. (*B*, *Right*) Effect of TCB-2 (0.1–10 μM) on the driving force (control, $n = 12$; TCB-2, $n = 14$). *$P < 0.05$ (Mann–Whitney test); **$P < 0.01$ (Wilcoxon paired test). (*C*) Effect of TCB-2 (0.1 μM) on E_{IPSP} and the driving force of motoneurons (six and nine in the absence and in the presence of TCB-2, respectively) in animals with SCI at birth. ***$P < 0.001$, *$P < 0.05$ (Mann–Whitney test); *$P < 0.05$ (Wilcoxon paired test) ($n = 6$). (*D*) E_{IPSP} was significantly depolarized by the application of the KCC2 blocker VU0240551 (25 μM), which prevented the hyperpolarizing effect of TCB-2 (0.1 μM; $n = 11$). Averages are taken from 3 motoneurons in control situation, 9 motoneurons under VU0240551, and 11 motoneurons in the presence of both VU0240551 and TCB-2. ns, $P > 0.05$; **$P < 0.01$ (Mann–Whitney test). (*E*) TCB-2 (0.1 μM; 30 min) significantly increased the expression of KCC2 at the plasma membrane of Hb9::eGFP transgenic motoneurons in culture (14 DIV). (*E*, *Left* and *Center*) Merge images (*Insets*) show the KCC2 immunolabeling at the periphery of GFP-expressing cytosol. (*E*, *Right*) Ratio of KCC2 expression between plasma membrane and cytosol. ***$P < 0.001$ (*t* test; $n = 34$ cells from two experiments analyzed in each condition). (*F*) Preincubation of the PKC inhibitor chelerythrine (20 μM; 30 min; $n = 6$) prevented the effect of DOI (10 μM; $n = 3$; gray) or TCB-2 (0.1 μM; $n = 3$). PDBu significantly hyperpolarized E_{IPSP}. ns, $P > 0.05$; *$P < 0.05$ (Wilcoxon paired test). The Ca^{2+}-dependent PKC inhibitor Gö6976 (2 μM; $n = 8$) induced a slight but significant hyperpolarization of E_{IPSP} and a further ~4-mV negative shift was observed after adding TCB-2 (0.1 μM; $n = 16$). **$P < 0.001$ (Mann–Whitney test); *$P < 0.05$ (Wilcoxon paired test). The activator of the Ca^{2+}-independent PKCε (FR236924; 2–8 μM; $n = 7$) hyperpolarized E_{IPSP}. *$P < 0.05$ (Wilcoxon paired test).

E_{IPSP} switched from above to below V_{rest} (Fig. 2*C*; $P < 0.05$; Wilcoxon paired test).

The use of 5-HT$_{2A}$ antagonists (ketanserin at 1 μM and MDL11,939 at 2 μM) and 5-HT$_{2B/2C}$ agonists and antagonists confirmed the involvement of 5-HT$_{2A}$R in the negative shift of E_{IPSP} and suggested that 5-HT$_{2B/2C}$ may have opposite effects (Fig. S2). To identify the mechanisms underlying these effects, we used VU0240551 (25 μM), a highly specific KCC2 blocker (23). This compound depolarized E_{IPSP} by >10 mV (Fig. 2*D*). KCC2 blockade occluded the effect of TCB-2 (Fig. 2*D*, *Right*), which is consistent with the requirement of KCC2 for the E_{IPSP} shift induced by the activation of 5-HT$_{2A}$R. TCB-2 had no effect on the kinetics of IPSPs (Fig. S3), indicating that it modulates the strength of inhibition essentially through a modulation of KCC2 function.

We used immunolabeling to quantify the effect of TCB-2 on the expression of KCC2 at the plasma membrane of cultured motoneurons isolated from Hb9::eGFP transgenic mice (Fig. 2*E*, *Left*). Following activation of 5-HT$_{2A}$R by TCB-2 (0.1 μM; 30 min), the ratio of KCC2 expression between plasma membrane and cytosol, visualized by eGFP fluorescence (Fig. 2*E*, *Insets*), was strongly increased (Fig. 2*E*, *Right*).

PKC-Dependent Pathway Is Involved. We next investigated the second messenger pathway activated by TCB-2/DOI. 5-HT$_{2A}$Rs stimulate phospholipase C, leading to activation of PKC. Consistent with an involvement of PKC, the effects of both TCB-2 (Fig. 2*F*, black) and DOI (Fig. 2*F*, gray) were prevented by preincubation of PKC inhibitor chelerythrine (20 μM). In addition, activation of PKC with phorbol 12,13-dibutyrate (PDBu) (1 μM) induced an ~9-mV negative shift of E_{IPSP} (Fig. 2*F*), which switched on average from above (5.5 ± 3.7 mV) to below (−3.3 ± 2.1 mV) V_{rest}. PKCs are divided into subfamilies, based on their second messenger requirements. The indolocarbazole Gö6976 enables discrimination between Ca^{2+}-dependent and -independent isoforms of PKC. Nanomolar concentrations of this compound inhibit the Ca^{2+}-dependent isozymes, whereas even micromolar concentrations have no effect on the Ca^{2+}-independent PKC subtypes (24). Gö6976 (2 μM) induced a small (~1.5 mV) but significant hyperpolarization of E_{IPSP} (Fig. 2*F*). Importantly, a further ~4-mV negative shift was observed after adding TCB-2 (Fig. 2*F*). The potent and selective activator of the Ca^{2+}-independent PKCε, FR236924, induced an ~2-mV negative shift of E_{IPSP} (Fig. 2*F*). Altogether, these results demonstrate that the activation of 5-HT$_{2A}$R increases KCC2 function, at least in part, through a Ca^{2+}-independent PKC.

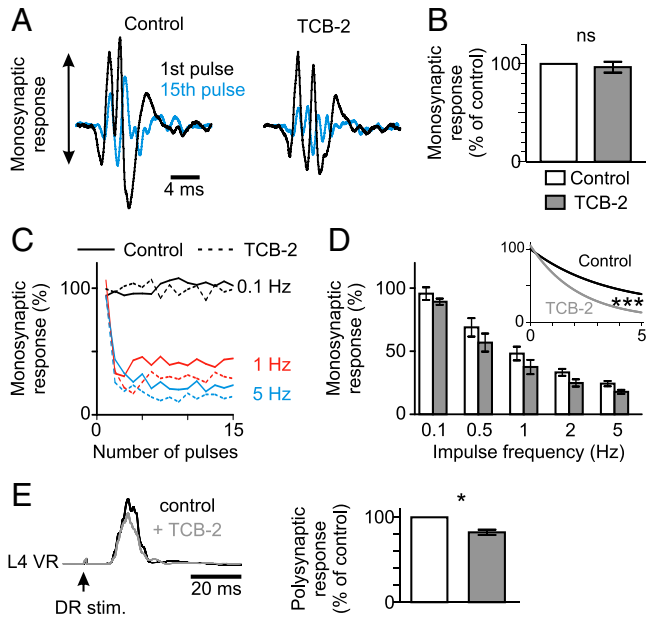

Fig. 3. Effects of TCB-2 on ventral root responses to dorsal root stimulation in the intact spinal cord in vitro. (*A*) Responses evoked in the L5 ventral root by supramaximal stimulation of the ipsilateral homonymous dorsal root, in the in vitro spinal cord isolated from rats at P6. The earliest component represents the monosynaptic response of motoneurons. The amplitude of this response decreased when the dorsal root was stimulated repeatedly (response to the 15th pulse at 1 Hz is shown in blue, superimposed with the control response to the first pulse). The slight increase in latency is attributable to a delayed firing of motoneurons as the pulse number increases. The amplitude of the response to the 15th pulse was much smaller after adding TCB-2 (0.1–0.15 μM). (*B*) Relative amplitudes of the monosynaptic responses delivered every 30 s before and 20–30 min after adding TCB-2 [percentage of control before TCB-2; $P > 0.05$ (Wilcoxon paired test); $n = 12$]. (*C*) Relative amplitudes of the monosynaptic responses to 15 consecutive stimulations at different frequencies (0.1 Hz, black; 1 Hz, red; 5 Hz, blue) before (continuous line) and after adding TCB-2 (dotted line). This is the same experiment as in *A*. (*D*) Mean (± SEM) relative amplitudes of the monosynaptic reflex at different stimulation frequencies in seven animals at P5–P6 before [controls in artificial cerebrospinal fluid (aCSF)] and after TCB-2 application (0.1–0.15 μM). Twelve values (the first three discarded) were averaged for each animal. The RDD was significantly increased by TCB-2. ***$P < 0.001$ (one-phase exponential decay regression). Note that for each frequency of stimulation, except at 0.1 Hz, the difference between before and after TCB-2 was significant [$P < 0.05$ (Wilcoxon paired test)]. (*E*) Mean envelopes of the ventral root (VR) burst evoked by stimulation of the ipsilateral homonymous dorsal root (DR) before and after adding TCB-2 (0.15 μM). *$P < 0.05$ (Wilcoxon paired test; $n = 7$).

Activation of 5-HT_{2A}R Increases the Strength of Inhibition. Supramaximal stimulation of a lumbar dorsal root elicits a response in the homonymous ipsilateral ventral root in vitro (Fig. 3*A*). The earliest component representing the monosynaptic excitation of motoneurons (25, 26) was not affected by TCB-2 (0.1–0.15 μM; Fig. 3 *A* and *B*). The amplitude of the monosynaptic response decreases when the dorsal root is stimulated repeatedly (Fig. 3*A*), an effect that gets stronger as the frequency of stimulation increases [rate-dependent depression (RDD); Fig. 3*C*]. Because KCC2 plays a key role in the depression of the response (Fig. S4), we hypothesized that hyperpolarizing E_{IPSP} by TCB-2 would affect the RDD. As expected, TCB-2 reduced the amplitude of the monosynaptic response elicited by repetitive stimulation (Fig. 3 *A*, blue trace, and Fig. 3*C*, dotted lines). As a result, the RDD was significantly increased (Fig. 3*D*). This effect was prevented by VU0240551 (Fig. S5).

We next considered the polysynaptic response, which results from a mixture of excitation and inhibition in motoneurons (27, 28). The polysynaptic response is potentiated by VU0240551 within 15–20 min, as a result of decreased strength of inhibition (Fig. S6). This effect was reversible. TCB-2 reduced the polysynaptic response within 15–20 min, and this effect lasted at least 1 h (Fig. 3*E*), an effect that was occluded by prior application of picrotoxin and strychnine (to block $GABA_A$Rs and GlyRs, respectively) or VU0240551 (Fig. S6). Therefore, TCB-2 increases the strength of postsynaptic inhibition in the intact spinal cord in vitro likely through a modulation of chloride homeostasis. In addition, such strengthening of inhibition by TCB-2 enabled to restore the alternating locomotor pattern that is disorganized after neonatal SCI (15) (Fig. S7).

Reduction of Spasticity After SCI. The H (or Hoffmann) reflex is commonly used to assess the excitability of the monosynaptic reflex loop in individuals suffering from spasticity. The H wave (Fig. 4*A*) resulting from the monosynaptic activation of motoneurons by type Ia afferents undergoes an RDD when using frequencies of stimulation higher than 0.1 Hz (29) (Fig. 4 *A*–*C*). Reduction of the RDD is a reliable correlate of spasticity after SCI (10, 29, 30). The down-regulation of KCC2 accounts, at least in part, for this reduction (10). We investigated the effects of TCB-2 (0.3 mg/kg, i.p.) on the RDD in paraplegic spastic adult rats (14–21 d post-SCI). The RDD remained quite stable after i.p. injection of the vehicle (NaCl; Fig. 4 *B* and *C*). Injection of TCB-2 did not affect the thresholds, maximal amplitudes, or stimulus intensities at which the maximal amplitude is obtained for both M and H waves at 0.1 Hz (Table S2). However, an effect was clearly present when frequencies of stimulation higher than 0.5 Hz were used (Fig. 4 *B* and *C*). Indeed, the amplitude of the H wave was smaller than it was before injection, with a maximal and highly significant effect 7–25 min after TCB-2 injection (Fig. 4 *B* and *C*).

Discussion

This study demonstrates that the activation of a receptor to a neurotransmitter restores endogenous inhibition in pathological conditions by up-regulating KCC2 function. Activation of 5-HT_{2A}R by TCB-2 in vitro leads to a hyperpolarizing shift of E_{IPSP} and an increased cell surface expression of KCC2 within minutes. Blocking KCC2 occluded this shift, indicating that the effect of TCB-2 is likely mediated by posttranslational modification of KCC2, as opposed to changes in gene transcription or protein synthesis. Chronic activation of 5-HT_{2A}R also induced a hyperpolarizing shift of E_{IPSP} and a concomitant increased expression of KCC2. Changes in gene transcription or protein synthesis may occur in this situation, as suggested by the trend toward an increase in cytoplasmic KCC2.

Modulation of chloride homeostasis by 5-HT has been previously reported in the spinal cord [in zebrafish (31)] and several other systems (e.g., refs. 32 and 33). Here, we showed that the effect of 5-HT_{2A}R activation on chloride homeostasis was critically dependent on PKC. In agreement with these findings, the activity of a number of protein kinases, including PKC and phosphatases, has been reported to influence KCC2 function. It was further demonstrated that KCC2 is directly phosphorylated by PKC activity and that the major site of phosphorylation within the C-terminal intracellular domain of this protein is serine 940 (Ser940). PKC-dependent phosphorylation of Ser940 increases KCC2 cell surface stability and activity by decreasing endocytosis from the plasma membrane (13). In HEK-293 cells, the entire cell surface population of KCC2 is internalized over a time course of 10 min, a process that is dramatically slowed by activation of PKC (13). Similarly, in cultured hippocampal neurons, PKC activation increases the cell surface expression of KCC2.

Activation of 5-HT_{2A}R still induced a hyperpolarizing shift of E_{IPSP} after blocking Ca^{2+}-dependent PKC by Gö6976. In addition, this compound induced a small hyperpolarizing shift of E_{IPSP}. These results suggest opposite effects of Ca^{2+}-dependent and Ca^{2+}-independentxPKC on KCC2 function. In support of this

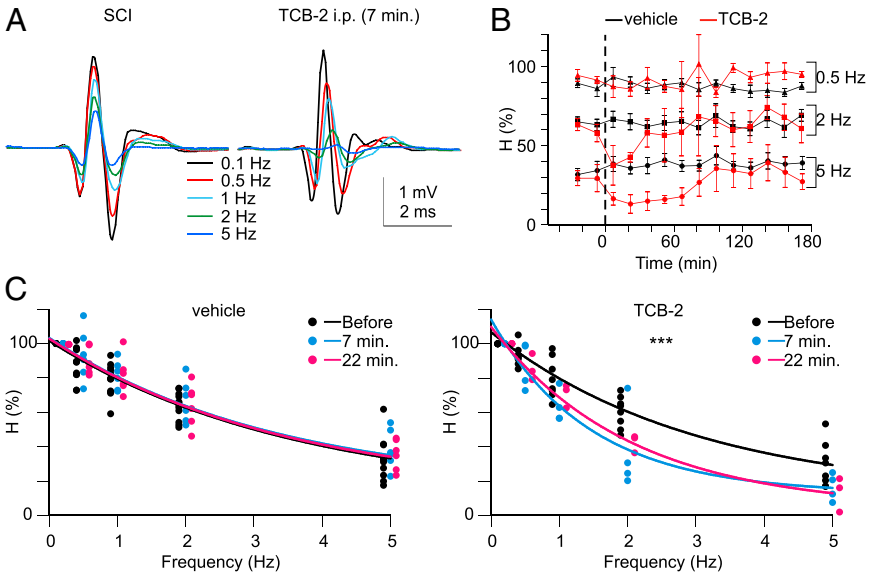

Fig. 4. Activation of 5-HT_{2A}Rs increases the RDD of the H reflex. (*A*) H_{max} responses evoked in adult rats after SCI before (*Left*) and 7 min after i.p. injection of TCB-2 (0.3 mg/kg) (*Right*). Each trace is the mean response to 17 consecutive stimulations (the first three discarded) at 0.1, 0.5, 1, 2, or 5 Hz. (*B*) Time course of the change in H-reflex depression after i.p. injection of vehicle (NaCl; $n = 6$ rats) or TCB-2 ($n = 4$). (*C*) Mean relative amplitudes of the H reflex before (black) and after (blue, 7 min; red, 22 min) the injection of vehicle (*Left*) or TCB-2 (*Right*). The data of all experiments are represented (the dots that are slightly offset at each frequency of stimulation are for clarity) together with the one-phase exponential decay fit of these data. ***$P < 0.001$, comparison of the fits before and after TCB-2 (either 7 or 22 min). The fits before and after vehicle are not significantly different.

hypothesis, repetitive postsynaptic spiking induces a positive shift in E_{Cl} through a Ca^{2+}-dependent down-regulation of KCC2 (34-36). Inhibition of Ca^{2+}-dependent PKC abolishes the spiking-induced shift in E_{Cl} (34). In agreement with a negative effect of intracellular Ca^{2+} on KCC2 function, NMDA receptor activation leads to Ca^{2+} influx that ultimately causes protein phosphatase 1–mediated dephosphorylation of KCC2 residue Ser940 and depolarizing shift of E_{Cl} (37).

We showed that blocking 5-HT_{2B}Rs and 5-HT_{2C}Rs hyperpolarized E_{IPSP}. Conversely, activating these receptors induced a depolarizing shift of E_{IPSP}. Although we did not determine whether these effects are mediated by one or both of these receptors, these results suggest that 5-HT_{2A}Rs and 5-$HT_{2B/2C}$Rs have opposite effects on KCC2 function. Although the pharmacological characteristics of 5-HT_{2A}Rs and 5-HT_{2C}Rs are quite similar, owing, in part, to the high level of amino acid sequence homology between them (38), significant differences have been reported between the signaling cascades regulated by these receptors (39, 40). Consistent with these observations, 5-HT_{2A}Rs and 5-HT_{2C}Rs exert opposing effects on both locomotor activity in mice (41) and the long-lasting amplification of spinal reflexes in rats (42). Interestingly, 5-HT_{2B}Rs and 5-HT_{2C}Rs become constitutively active (spontaneously active without 5-HT) after SCI (43, 44). This constitutive activity may be partly responsible for the depolarizing shift of E_{Cl} after SCI (10). The modulatory effects of 5-$HT_{2B/2C}$Rs on chloride homeostasis require furtherinvestigation.

The activation of 5-HT_{2A}R reduced spasticity after SCI, as revealed by the increased RDD of the H reflex. This effect was very likely due to the restoration of endogenous inhibition, because slight changes in E_{Cl} were shown to have an important impact on the strength of inhibition (5–7, 10). 5-HT_{2A}Rs are strongly expressed in the ventral horn (45) and are mainly localized in the plasma membrane of neurons, covering a large surface of cell bodies and dendrites (46). These receptors are dramatically up-regulated in the motoneuron somata and dendrites following SCI (47), an effect that starts as early as 1 d after transection (48). The 5-HT_{2A}R displays ~10-fold lower constitutive activity than the 5-HT_{2C}R (38).

In the intact spinal cord, the neuromodulators released by descending pathways allow the motoneurons to exhibit sustained depolarizations (plateau potentials), which are attributable to slowly activating voltage-dependent persistent inward currents (PICs). Shortly after the injury, the excitability of the spinal cord decreases because this excitatory influence of the brainstem on motoneurons is lost. However, motoneurons slowly recover the capacity to generate PICs, which are, in large part, responsible for long-lasting reflexes and spasms (49, 50). Both 5-HT_{2B}Rs and 5-HT_{2C}Rs, but not 5-HT_{2A}Rs, are involved in this up-regulation of PICs (44). To conclude, by restoring endogenous inhibition through an up-regulation of KCC2 function, without depolarizing motoneurons and activating PICs, activation of 5-HT_{2A}Rs may represent an innovative therapeutic strategy to reduce spasticity after SCI. However, these receptors have been implicated in several psychiatric disorders (e.g., 51), and their effects on pain processing are controversial (52), highlighting the need to further investigate the potential systemic effects of specific 5-HT_{2A}R agonists, such as TCB-2.

Materials and Methods

In Vitro Electrophysiological Recordings. After hypothermic anesthesia, we dissected out the spinal cords (sacral segments up to T8–T9) and L3–L5 dorsal and ventral roots of newborn rats. Dissections and electrophysiological procedures were performed under continuous perfusion with an oxygenated artificial CSF.

In Vivo Electrophysiological Recordings. We measured the H reflex in adult rats under ketamine anesthesia (100 mg/kg, i.p.) using a pair of stainless steel needle electrodes transcutaneously inserted into the vicinity of the tibial nerve for stimulation. We placed the recording electrode into the flexor digitorum muscle beneath the ankle and the reference electrode s.c. into the foot.

Western Blots. The amount of KCC2 in the lumbar enlargement of the spinal cord was determined by Western blots as described previously (10). The procedures used for separating membrane and cytoplasmic fractions are detailed in *SI Materials and Methods*.

Immunohistochemistry. Fast blue (FB) [3 μL; 0.5% in 0.9% NaCl; F-5756 (Sigma)] was injected bilaterally in the TS muscles (ankle extensors) anesthetized animals at P5 for retrograde identification. Animals were killed 2 d later. After fixation, spinal cords were cut transversally (20-μm-thick sections). Immunohistochemistry was performed by using a mixture of affinity-purified rabbit

KCC2-specific polyclonal antibody and GlyR monoclonal antibody. We then revealed the labeling with a mixture of donkey Cy3-conjugated rabbit-specific antibody and donkey AlexaFluor 488–conjugated mouse-specific antibody.

Motoneuron Cultures and Immunocytochemistry. Motoneurons were isolated and cultured. At 13–14 d in vitro (DIV), TCB-2 was freshly prepared, diluted in complete culture medium (0.1 μM), and added for 30 min.

Further experimental details are given in *SI Materials and Methods*.

ACKNOWLEDGMENTS. We thank Mouloud Bouhadfane for helpful discussions throughout the experiments and Florian Gackière and Frédéric Brocard for their comments on the manuscript. This work was supported by the Christopher and Dana Reeve Foundation Grants VB1-0502-2 and VB2-0801-2, the International Spinal Research Trust Grant STR110, the French Agence Nationale pour la Recherche Grant ANR-2010-BLAN-1407-01, and the French Institut pour la Recherche sur la Moelle épinière et l'Encéphale (to L.V.). P.B., G.H., and H.B. are supported by the Institut National de la Santé et de la Recherche Médicale, and K.S. is supported by Association Française contre les Myopathies Grant 13912.

1. Blaesse P, Airaksinen MS, Rivera C, Kaila K (2009) Cation-chloride cotransporters and neuronal function. *Neuron* 61(6):820–838.
2. Payne JA, Stevenson TJ, Donaldson LF (1996) Cation-chloride co-transporters in neuronal communication, development and trauma. *J Biol Chem* 271(27):16245–16252.
3. Payne JA, Rivera C, Voipio J, Kaila K (2003) Molecular characterization of a putative K-Cl cotransporter in rat brain. A neuronal-specific isoform. *Trends Neurosci* 26(4):199–206.
4. Kahle KT, et al. (2008) Roles of the cation-chloride cotransporters in neurological disease. *Nat Clin Pract Neurol* 4(9):490–503.
5. Jean-Xavier C, Mentis GZ, O'Donovan MJ, Cattaert D, Vinay L (2007) Dual personality of GABA/glycine-mediated depolarizations in immature spinal cord. *Proc Natl Acad Sci USA* 104(27):11477–11482.
6. Doyon N, et al. (2011) Efficacy of synaptic inhibition depends on multiple, dynamically interacting mechanisms implicated in chloride homeostasis. *PLOS Comput Biol* 7(9): e1002149.
7. Prescott SA, Sejnowski TJ, De Koninck Y (2006) Reduction of anion reversal potential subverts the inhibitory control of firing rate in spinal lamina I neurons: Towards a biophysical basis for neuropathic pain. *Mol Pain* 2:32.
8. Biering-Sørensen F, Nielsen JB, Klinge K (2006) Spasticity-assessment: A review. *Spinal Cord* 44(12):708–722.
9. Boulenguez P, Vinay L (2009) Strategies to restore motor functions after spinal cord injury. *Curr Opin Neurobiol* 19(6):587–600.
10. Boulenguez P, et al. (2010) Down-regulation of the potassium-chloride cotransporter KCC2 contributes to spasticity after spinal cord injury. *Nat Med* 16(3):302–307.
11. Cramer SW, et al. (2008) The role of cation-dependent chloride transporters in neuropathic pain following spinal cord injury. *Mol Pain* 4:36.
12. Lu Y, Zheng J, Xiong L, Zimmermann M, Yang J (2008) Spinal cord injury-induced attenuation of GABAergic inhibition in spinal dorsal horn circuits is associated with down-regulation of the chloride transporter KCC2 in rat. *J Physiol* 586(Pt 23):5701–5715.
13. Lee HH, et al. (2007) Direct protein kinase C-dependent phosphorylation regulates the cell surface stability and activity of the potassium chloride cotransporter KCC2. *J Biol Chem* 282(41):29777–29784.
14. Pearlstein E, Ben Mabrouk F, Pflieger JF, Vinay L (2005) Serotonin refines the locomotor-related alternations in the *in vitro* neonatal rat spinal cord. *Eur J Neurosci* 21(5):1338–1346.
15. Norreel JC, et al. (2003) Reversible disorganization of the locomotor pattern after neonatal spinal cord transection in the rat. *J Neurosci* 23(5):1924–1932.
16. Jordan LM, Sławińska U (2011) Chapter 12—modulation of rhythmic movement: Control of coordination. *Prog Brain Res* 188:181–195.
17. Grillner S (2003) The motor infrastructure: From ion channels to neuronal networks. *Nat Rev Neurosci* 4(7):573–586.
18. Kiehn O (2006) Locomotor circuits in the mammalian spinal cord. *Annu Rev Neurosci* 29:279–306.
19. Jean-Xavier C, Pflieger JF, Liabeuf S, Vinay L (2006) Inhibitory postsynaptic potentials in lumbar motoneurons remain depolarizing after neonatal spinal cord transection in the rat. *J Neurophysiol* 96(5):2274–2281.
20. Sadlaoud K, et al. (2010) Differential plasticity of the GABAergic and glycinergic synaptic transmission to rat lumbar motoneurons after spinal cord injury. *J Neurosci* 30(9):3358–3369.
21. McLean TH, et al. (2006) 1-Aminomethylbenzocycloalkanes: Conformationally restricted hallucinogenic phenethylamine analogues as functionally selective 5-HT2A receptor agonists. *J Med Chem* 49(19):5794–5803.
22. Fox MA, French HT, LaPorte JL, Blackler AR, Murphy DL (2010) The serotonin 5-HT(2A) receptor agonist TCB-2: A behavioral and neurophysiological analysis. *Psychopharmacology (Berl)* 212(1):13–23.
23. Delpire E, et al. (2009) Small-molecule screen identifies inhibitors of the neuronal K-Cl cotransporter KCC2. *Proc Natl Acad Sci USA* 106(13):5383–5388.
24. Martiny-Baron G, et al. (1993) Selective inhibition of protein kinase C isozymes by the indolocarbazole Gö 6976. *J Biol Chem* 268(13):9194–9197.
25. Fulton BP, Walton K (1986) Electrophysiological properties of neonatal rat motoneurones studied in vitro. *J Physiol* 370:651–678.
26. Lev-Tov A, Pinco M (1992) In vitro studies of prolonged synaptic depression in the neonatal rat spinal cord. *J Physiol* 447:149–169.
27. Wallis DI, Wu J (1992) FAST and SLOW ipsilateral and contralateral spinal reflexes in the neonate rat are modulated by 5-HT. *Gen Pharmacol* 23(6):1035–1044.
28. Jiang Z, Carlin KP, Brownstone RM (1999) An in vitro functionally mature mouse spinal cord preparation for the study of spinal motor networks. *Brain Res* 816(2):493–499.
29. Thompson FJ, Reier PJ, Lucas CC, Parmer R (1992) Altered patterns of reflex excitability subsequent to contusion injury of the rat spinal cord. *J Neurophysiol* 68(5):1473–1486.
30. Grey MJ, et al. (2008) Post-activation depression of soleus stretch reflexes in healthy and spastic humans. *Exp Brain Res* 185(2):189–197.
31. Brustein E, Drapeau P (2005) Serotoninergic modulation of chloride homeostasis during maturation of the locomotor network in zebrafish. *J Neurosci* 25(46):10607–10616.
32. Mayer SE, Sanders-Bush E (1994) 5-Hydroxytryptamine type 2A and 2C receptors linked to Na+/K+/Cl- cotransport. *Mol Pharmacol* 45(5):991–996.
33. Broadbelt KG, Paterson DS, Rivera KD, Trachtenberg FL, Kinney HC (2010) Neuroanatomic relationships between the GABAergic and serotonergic systems in the developing human medulla. *Auton Neurosci* 154(1-2):30–41.
34. Fiumelli H, Cancedda L, Poo MM (2005) Modulation of GABAergic transmission by activity via postsynaptic Ca2+-dependent regulation of KCC2 function. *Neuron* 48(5): 773–786.
35. Woodin MA, Ganguly K, Poo MM (2003) Coincident pre- and postsynaptic activity modifies GABAergic synapses by postsynaptic changes in Cl- transporter activity. *Neuron* 39(5):807–820.
36. Fiumelli H, Woodin MA (2007) Role of activity-dependent regulation of neuronal chloride homeostasis in development. *Curr Opin Neurobiol* 17(1):81–86.
37. Lee HH, Deeb TZ, Walker JA, Davies PA, Moss SJ (2011) NMDA receptor activity downregulates KCC2 resulting in depolarizing GABAA receptor-mediated currents. *Nat Neurosci* 14(6):736–743.
38. Aloyo VJ, Berg KA, Spampinato U, Clarke WP, Harvey JA (2009) Current status of inverse agonism at serotonin2A (5-HT2A) and 5-HT2C receptors. *Pharmacol Ther* 121(2): 160–173.
39. Berg KA, Clarke WP, Sailstad C, Saltzman A, Maayani S (1994) Signal transduction differences between 5-hydroxytryptamine type 2A and type 2C receptor systems. *Mol Pharmacol* 46(3):477–484.
40. Berg KA, Stout BD, Maayani S, Clarke WP (2001) Differences in rapid desensitization of 5-hydroxytryptamine2A and 5-hydroxytryptamine2C receptor-mediated phospholipase C activation. *J Pharmacol Exp Ther* 299(2):593–602.
41. Halberstadt AL, et al. (2009) 5-HT(2A) and 5-HT(2C) receptors exert opposing effects on locomotor activity in mice. *Neuropsychopharmacology* 34(8):1958–1967.
42. Machacek DW, Garraway SM, Shay BL, Hochman S (2001) Serotonin 5-HT(2) receptor activation induces a long-lasting amplification of spinal reflex actions in the rat. *J Physiol* 537(Pt 1):201–207.
43. Murray KC, et al. (2010) Recovery of motoneuron and locomotor function after spinal cord injury depends on constitutive activity in 5-HT2C receptors. *Nat Med* 16(6):694–700.
44. Murray KC, Stephens MJ, Ballou EW, Heckman CJ, Bennett DJ (2011) Motoneuron excitability and muscle spasms are regulated by 5-HT2B and 5-HT2C receptor activity. *J Neurophysiol* 105(2):731–748.
45. Pearlstein E, Bras H, Deneris ES, Vinay L (2011) Contribution of 5-HT to locomotion - the paradox of Pet-1(-/-) mice. *Eur J Neurosci* 33(10):1812–1822.
46. Doly S, et al. (2004) The 5-HT2A receptor is widely distributed in the rat spinal cord and mainly localized at the plasma membrane of postsynaptic neurons. *J Comp Neurol* 472(4):496–511.
47. Kong XY, Wienecke J, Hultborn H, Zhang M (2010) Robust upregulation of serotonin 2A receptors after chronic spinal transection of rats: An immunohistochemical study. *Brain Res* 1320:60–68.
48. Kong XY, Wienecke J, Chen M, Hultborn H, Zhang M (2011) The time course of serotonin 2A receptor expression after spinal transection of rats: An immunohistochemical study. *Neuroscience* 177:114–126.
49. Bennett DJ, Sanelli L, Cooke CL, Harvey PJ, Gorassini MA (2004) Spastic long-lasting reflexes in the awake rat after sacral spinal cord injury. *J Neurophysiol* 91(5):2247–2258.
50. Gorassini MA, Knash ME, Harvey PJ, Bennett DJ, Yang JF (2004) Role of motoneurons in the generation of muscle spasms after spinal cord injury. *Brain* 127(Pt 10):2247–2258.
51. González-Maeso J, Sealfon SC (2009) Psychedelics and schizophrenia. *Trends Neurosci* 32(4):225–232.
52. Millan MJ (2002) Descending control of pain. *Prog Neurobiol* 66(6):355–474.
53. Blaesse P, et al. (2006) Oligomerization of KCC2 correlates with development of inhibitory neurotransmission. *J Neurosci* 26(41):10407–10419.

Supporting Information

Bos et al. 10.1073/pnas.1213680110

SI Materials and Methods

Animals. *Wistar* rats were purchased from Janvier. Hb9::eGFP and *Slc12a5*$^{+/-}$ transgenic mice were kindly provided by T. Jessel (Columbia University, New York, NY) and E. Delpire (Vanderbilt University Medical Center, Nashville, TN), respectively. Animals were housed in a temperature-controlled animal care facility with a 12 h light–dark cycle. Generation and genotyping of the transgenic mice used have been described previously (1). We made all efforts to minimize animal suffering and the number of animals used. We performed experiments in accordance with French regulations (Ministry of Food, Agriculture and Fisheries, Division of Health and Protection of Animals). The local Direction of Veterinary Services and Ethical Committee (Marseille, Provence) delivered the appropriate licenses and approved the protocols, respectively.

Surgery. We anesthetized female rats (220–280 g) with a mixture of ketamine (60 mg/kg, i.p.; Imalgene; Merial) and medetomidine (0.25 mg/kg, i.p.; Domitor; Pfizer) and neonates by hypothermia. Amoxicillin, a long-lasting antibiotic, was administered immediately after anesthesia (150 mg/kg, s.c.; Clamoxyl LA; Pfizer). After laminectomy, we transected the spinal cord at the thoracic level (T8–T9). We treated sham-operated animals in the same way except for the spinal cord transection. Postsurgical care and treatments are described below. The surgery for transecting the spinal cord in neonates was similar to that described previously (2–4).

Postsurgical Treatments and Care of the Animals. After SCI in adult rats, we injected 5 mL of NaCl s.c., kept the rats warm until awakening, and placed some food with glucose in the cage. We administered buprenorphine to the rats every 8 h for 24 h (0.05 mg/kg, s.c.; Temgesic; Reckitt Benckiser Healthcare) and diluted DL-lysine acetylsalicylate in their drinking water for 3 d (200 mg in 150 mL of drinking water; Aspégic nourissons; Sanofi Aventis). Twice a day, we manually emptied their bladders until recovery of the urinary function, checked their temperature and hydration, and observed any clinical sign of pain or infection. No urinary infection occurred. We killed rats presenting a more than 20% decrease in body weight, a temperature under 35 °C, or signs of autophagia with a lethal dose of pentobarbital.

Chronic Pharmacological Treatment. We activated 5-HT$_2$Rs in animals with a SCI at birth by daily i.p. administration of the 5-HT$_2$R agonist DOI, from P4 to P6–P7 [0.15 mg/kg DOI diluted in 50 μL of NaCl (2, 4)]. Sham-treated animals were injected with 50 μL of NaCl only.

Western Blot. We euthanized animals by decapitation and quickly dissected out and froze T8-sacral parts of the spinal cords. For each sample, two spinal cords were pooled. For cytoplasmic and membrane fractions, we homogenized samples in cold lysis buffer B (described below) without detergent and centrifuged them first at 7,000 × *g* for 5 min and then at 18,000 × *g* for 70 min at 4 °C. We collected pellets (membrane-enriched fractions) in lysis buffer A and supernatants (cytoplasmic fractions). We determined supernatant protein concentrations using a detergent-compatible protein assay (Bio-Rad). We then immunoprecipitated KCC2 (described below), separated samples in 6% (vol/vol) SDS/PAGE from 40% Acryl/Bisacrylamide (29/1) commercial solution, and transferred them to a PVDF membrane. After blockade in Tris-buffered saline–5% nonfat dry milk, we exposed membranes overnight at 4 °C to a polyclonal rabbit KCC2-specific antibody diluted at 1:700 (Millipore) in the blocking solution. The specificity of the KCC2 antibody to KCC2 is confirmed by the lower intensity of the signal in *Slc12a5*$^{+/-}$ and *Slc12a5*$^{-/-}$ mice (5). We used an ImmunoPure goat HRP-conjugated rabbit-specific antibody (1:120,000 in blocking solution; 1 h at 22 °C; Pierce Biotech) for chemiluminescent detection (Millipore). Signal intensities were measured with the image analysis software Quantity-One (Bio-Rad).

Composition of lysis buffer A. The composition of buffer A was 1% Igepal CA-630, 0.1% SDS, 10 mM sodium vanadate, 10 mM sodium fluoride, 10 mM sodium pyrophosphate, 10 mM iodoacetamide, and a mixture of protease inhibitors (CompleteMini; Roche Diagnostics).

Composition of lysis buffer B. The composition of buffer B was sucrose 320 mM in Tris-HCl (pH 7.5), 10 mM sodium vanadate, 10 mM sodium fluoride, 10 mM sodium pyrophosphate, 10 mM iodoacetamide, and a mixture of protease inhibitors.

KCC2 immunoprecipitation. We incubated the same amount of protein with an affinity-purified rabbit KCC2-specific polyclonal antibody (Millipore) for 4 h at 4 °C and precipitated the protein–antibody complexes with PureProteome protein G magnetic beads (Millipore). After several washes in lysis buffer, beads were resuspended in SDS sample buffer.

Immunohistochemistry and Quantification of KCC2 Labeling. For immunohistochemistry, we anesthetized the animals at P7 by hypothermia, and killed them by decapitation (n = 3 in each group). We rapidly excised the lumbar spinal cord, immersed it for 1 h in 20% sucrose, and embedded it in capsules filled with Tissutech (Sakura) quickly frozen by immersion in ethanol 100% kept at –80 °C. We cut transverse spinal cord sections (20 μm thick) with a cryostat (Microm) and mounted them onto gelatinized slides. We immersed section in 2% paraformaldehyde in 0.15 M PBS (pH 7.4) for 30 min and rinsed in PBS. We incubated sections overnight at 4 °C in a mixture of affinity-purified rabbit KCC2-specific polyclonal antibody (1:200; Millipore) and GlyR monoclonal antibody (mAb2b; 1:100; Synaptic Systems). We then revealed the labeling with a mixture of donkey Cy3-conjugated rabbit-specific antibody (1:500; Jackson Immunoresearch) and donkey AlexaFluor 488–conjugated mouse-specific antibody (1:800, Molecular Probes; 1 h at 22 °C) and mounted coverslips with a gelatinous aqueous medium. We analyzed the patterns of immunolabeling by means of a laser scanning confocal microscope (SM 510 META; Zeiss) at low (20×) or high magnification ([63× 1.4 (NA) oil immersion objective; Plan Apochromat].

Triple-fluorescent labelings were captured using frame-channel mode to avoid any cross-talk between the channels. Each optical section resulted from two scanning averages. Excitation of the fluorochromes was performed with a diode laser set at 405 nm to detect FB, an argon ion laser set at 488 nm, and a helium/neon laser set at 575 nm. At high magnification, we only scanned FB-retrogradely labeled TS motoneurons with visible nuclei, and for each soma, we digitized stacks of 1-μm-thick optical sections. Because the developmental up-regulation of GlyR is not affected by neonatal transaction (2), we used the GlyR immunolabeling to delimit the somatic membrane of the motoneurons in sham-operated, transected, and DOI-treated transected animals, respectively. We overlaid the internal and external borders and digitized intensity measurements of KCC2 labeling using the Fluoview software (Version 5; Olympus). To quantify KCC2 labeling in the dendrites, we framed a zone of the white matter underneath the IX layers of Rexed laminae. We used the nonparametric one-way ANOVA

(Kruskal–Wallis) with a Dunn's post test for multiple comparisons between sham animals and SCI and/or SCI-pharmacologically treated rats.

Motoneuron Culture and Immunocytochemistry. Hb9::GFP transgenic mice were maintained as hemizygotes by crossing with nontransgenic female mice. Mice were housed in a conventional dark/light cycle (dark 1100 hours to 0900 hours) and positive vaginal plugs at 0900 hours were recorded as embryonic day (E)0. Motoneurons were isolated from E12 spinal cords essentially as described previously (6, 7). Motoneurons were seeded at a density of about 5.000 cells per well in four-well plates previously treated with polyornithine (Life Technologies) and laminin (Becton Dickinson). Motoneurons were cultured in Neurobasal medium supplemented with 2% (vol/vol) horse serum, 25 μM L-glutamate, 25 μM β-mercaptoethanol, 0.5 mM L-glutamine, 2% (vol/vol) B-27 (all from Life Technologies), and the neurotrophic factors BDNF (1 ng/mL; R&D Systems), ciliary neurotrophic factor (CNTF) (10 ng/mL; R&D Systems), and glial cell line-derived neurotrophic factor (GDNF) (100 pg/mL; Sigma). Half of the culture medium was replaced every 2 d.

At 13 or 14 DIV, cultures were incubated with TCB-2 or mock for 30 min at 37 °C in an incubator containing 5% CO_2 in a humidified air atmosphere. Cultures were fixed for 15 min by adding an equal volume of 7.4% (vol/vol) formaldehyde in PBS, washed and blocked in buffer containing PBS, 0.1% Triton X-100, 1% BSA, and 5% goat serum. Coverslips were incubated overnight at 4 °C with rabbit polyclonal anti-KCC2 antibodies (Millipore) at 1:300 in blocking buffer, washed with PBS, and incubated for 1 h with Cy3-conjugated anti-rabbit antibodies (Jackson Immunoresearch) diluted in blocking buffer. Coverslips were mounted in Vectashield/DAPI solution (Vector Labs) and examined with a confocal fluorescence microscope (60× oil objective; Fluoview; Olympus). Thirty-four randomly chosen cells per condition from two independent experimental series were imaged at 3× magnification using identical settings for laser power, photomultipliers, electronic gain, and offset. For each cell, plasma membrane and cytosol were manually delimited and fluorescence intensities in both areas were quantified using the Neuron J plugin of the ImageJ software (National Institutes of Health). The individuals performing data analysis were blind to the conditions of motoneurons.

In Vitro Electrophysiological Recordings. The aCSF used for perfusion was composed of 130 mM NaCl, 4 mM KCl, 3.75 mM $CaCl_2$, 1.3 mM $MgSO_4$, 0.58 mM NaH_2PO_4, 25 mM $NaHCO_3$, and 10 mM glucose and was oxygenated with 95% O_2 and 5% CO_2 (pH 7.4; temperature 24–25 °C).

Intracellular recordings. We measured the effects of various pharmacological compounds on the reversal potentials of IPSPs (3) (E_{IPSP}) from the spinal cord of intact and cord-transected rats (P5–P7). We also measured E_{IPSP} 4–6 d after transection or sham surgery performed at P0. After removing the pia, we recorded lumbar motoneurons intracellularly using glass microelectrodes filled with 2 M K-acetate (90- to 150-MΩ resistance). We recorded intracellular potentials in the discontinuous current–clamp (DCC) mode (Axoclamp 2B amplifier; Digidata 1200 interface; pClamp9 software; Axon Instruments). We considered only neurons exhibiting a stable (>15 min) resting membrane potential for analysis. We identified motoneurons in the L4–L5 segments by their antidromic response to ventral root stimulation. We used glass suction electrodes to stimulate the ipsilateral ventral funiculus at the L2–L3 level. Such stimulations induced $GABA_A$ R– and GlyR-mediated IPSPs (3, 8, 9) in the presence of 2-amino-5-phosphonovaleric acid (AP5) (50–100 μM) and 6-cyano-7-nitroquin-oxaline-2,3-dione (CNQX) (10 μM). We recorded IPSPs at various holding potentials (500-ms-long current pulses) and collected at least 20 values for each motoneuron. We measured and plotted amplitudes of IPSPs against holding potentials and obtained E_{IPSP} from the regression line (Prism Version 5; Graphpad).

Quantification of polysynaptic responses. We placed monopolar stainless steel electrodes in contact with the spinal roots and insulated them with Vaseline for stimulation and recording (P5–P7). We recorded L4–L5 ventral roots discharges by means of an AC-coupled amplifier (bandwidth: 70 Hz to 3 kHz) in response to the stimulation of the homonymous dorsal root (0.3 ms). Stimulations were delivered at supramaximal intensity every 60 s to avoid the synaptic depression described in this preparation. Once the signal was stable for at least 20 min, we added the pharmacological compound to be tested to the perfusion liquid for 20–30 min. We rectified signals and measured the areas under the curve from 3 to 100 ms after the onset of the monosynaptic signal (pClamp9 software). The effect of the drug was considered 20 min following bath application of the compound.

Measurement of RDD in vitro. We delivered supramaximal electrical stimulations (0.3-ms duration) to dorsal roots. We measured the amplitude of the monosynaptic response between the first positive and negative peaks. We delivered 15 stimulations at various frequencies (30 s between each series). We normalized the amplitude of responses (the first three discarded) to the controls evoked at 30-s intervals (mean of five pulses). We took into account at least three series of stimulations before and 20–30 min after the application of the compound.

Fictive locomotion. The coordination between opposite L3 ventral root bursts was investigated during fictive locomotion in six transected animals (4) (P5, $n = 3$; P6, $n = 3$). Fictive locomotion was elicited by bath application of *N*-methyl-D, L-aspartate (NMA) (12–16 μM). Analyses consisted in rectifying and integrating the recordings (time constant of 25 ms). A threshold function was used to determine bursts onset and termination. The threshold was usually set to ~30% of the peak value. The duration of motor bursts was measured, and the middle of bursts was considered to calculate the period (defined as the time between the midpoint of two consecutive bursts) and the phase relationships between the left and right bursts (defined as the time between the midpoint of a burst and that of the next burst in the contralateral root, divided by the period of the ongoing cycle). The coordination was evaluated by means of cross-correlation analysis (pClamp9 software; Axon Instruments). Phase data were multiplied by 360° to be analyzed by means of circular statistics (Oriana; Kovach Computing Services).

In Vivo Electrophysiological Recordings (H Reflex). We repeated a series of measurements throughout the experiment. First, we stimulated the tibial nerve for 0.2 ms at 0.2 Hz with increasing current intensities (until M_{max} was stabilized) and determined the intensity necessary to get a maximal H response. Then, we used this intensity for trains of 20 stimulations at 0.1, 0.5, 1, 2, and 5 Hz to measure the RDD, with at least 1-min intervals between each train of stimulations so that a whole series of measurements lasted about 15min. We added one third of the initial dose of anesthesia every 30 min and maintained the rat temperature around 37 °C. To determine the level of RDD at the different frequencies, we discarded responses to the first three stimulations necessary for the depression to occur and expressed all of the responses as percentages relative to the mean response at 0.2 Hz in the same series of measurements.

We injected the drug or its vehicle after two stable series of measurements and carried on measuring current–voltage (I/V) curves and RDD for 3 h.

Drugs. We purchased DOI hydrochloride, ketanserin tartrate, VU0240551, PDBu, α-methyl 5-HT, NMA, strychnine, and picrotoxin from Sigma. We purchased TCB-2, MDL11,939, SB206553 hydrochloride, chelerythrine chloride, Gö6976, and FR236924 (DCP-LA) from Tocris. DL-AP5 and CNQX were purchased from Abcam. All compounds were prepared in aCSF except

VU0240551, PDBu, α-methyl 5-HT, MDL11,939, SB206553 hydrochloride, chelerythrine chloride, Gö6976, and FR236924, which were diluted in DMSO (0.1% final concentration).

Statistical Analyses. Group measurements are expressed as means ± SEM. We used *t* tests to compare two groups and one- or two-way ANOVA to compare more than two groups, or corresponding nonparametric analyses when data were not normally distributed or when small samples (<20) were analyzed (Prism 5 software; Graphpad). Nonlinear regressions were performed to compare the levels of H-reflex depression at all stimulation frequencies tested in different groups. A logarithmic transformation of frequency values was also performed to enable linear regression analyses and comparison of slopes. Statistical tests used in each case are given in figure legends. The level of significance was set at $P < 0.05$.

1. Jiang Z, Carlin KP, Brownstone RM (1999) An in vitro functionally mature mouse spinal cord preparation for the study of spinal motor networks. *Brain Res* 816(2):493–499.
2. Sadlaoud K, et al. (2010) Differential plasticity of the GABAergic and glycinergic synaptic transmission to rat lumbar motoneurons after spinal cord injury. *J Neurosci* 30(9):3358–3369.
3. Jean-Xavier C, Pflieger JF, Liabeuf S, Vinay L (2006) Inhibitory postsynaptic potentials in lumbar motoneurons remain depolarizing after neonatal spinal cord transection in the rat. *J Neurophysiol* 96(5):2274–2281.
4. Norreel JC, et al. (2003) Reversible disorganization of the locomotor pattern after neonatal spinal cord transection in the rat. *J Neurosci* 23(5):1924–1932.
5. Stil A, et al. (2011) Contribution of the potassium-chloride co-transporter KCC2 to the modulation of lumbar spinal networks in mice. *Eur J Neurosci* 33(7):1212–1222.
6. Raoul C, et al. (2006) Chronic activation in presymptomatic amyotrophic lateral sclerosis (ALS) mice of a feedback loop involving Fas, Daxx, and FasL. *Proc Natl Acad Sci USA* 103(15):6007–6012.
7. Arce V, et al. (1999) Cardiotrophin-1 requires LIFRbeta to promote survival of mouse motoneurons purified by a novel technique. *J Neurosci Res* 55(1):119–126.
8. Bos R, Brocard F, Vinay L (2011) Primary afferent terminals acting as excitatory interneurons contribute to spontaneous motor activities in the immature spinal cord. *J Neurosci* 31(28): 10184–10188.
9. Boulenguez P, et al. (2010) Down-regulation of the potassium-chloride cotransporter KCC2 contributes to spasticity after spinal cord injury. *Nat Med* 16(3):302–307.

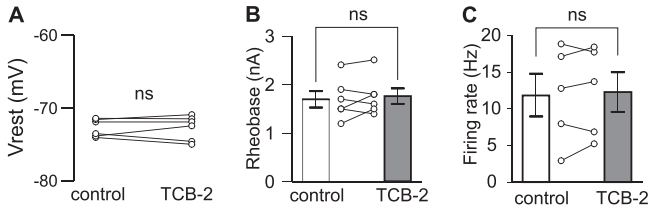

Fig. S1. TCB-2 has no effect on several electrical properties of motoneurons. (*A*) V_{rest} of six motoneurons (control rats; P5–P7) before and 20–30 min after starting bath application of TCB-2 (0.1 μM diluted in aCSF). (*B* and *C*) TCB-2 has a significant effect neither on the rheobase (defined as the minimum current required to induce action potential during a 500 ms pulse; $n = 5$) (*B*) nor on the firing rate ($n = 5$) (*C*). The firing rate was recorded at 1.5-twofold the rheobase in the both conditions. ns, $P > 0.05$ (Wilcoxon paired test).

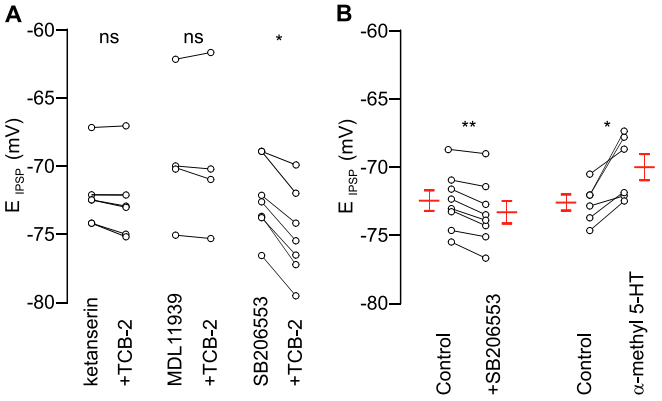

Fig. S2. Relative effects of blocking or activating 5-HT_{2A}R and 5-$HT_{2B/C}$R on E_{IPSP}. (*A*) Preincubation during 30 min of the 5-HT_2R antagonist ketanserin (1 μM; $n = 4$) or the more specific 5-HT_{2A}R antagonist MDL11,939 (2 μM; $n = 4$) prevented the hyperpolarizing effect of TCB-2 (0.1 μM) on E_{IPSP}. The latter compound had no effect on E_{IPSP} (−70.6 and −70.8 mV in control and under MDL11,939, respectively; $n = 4$). TCB-2 (0.1 μM) still induced a hyperpolarizing shift of E_{IPSP} in the presence of the 5-HT_{2B-C}R antagonist SB206553 (3–5 μM; $n = 6$). (*B*) Hyperpolarizing effect of the 5-$HT_{2B/2C}$R antagonist SB206553 (3–5 μM) on E_{IPSP} in motoneurons recorded from control rats (P5–P7; $n = 8$). E_{IPSP} was significantly more depolarized after application of the 5-$HT_{2B/2C}$R agonist α-methyl 5-HT (0.5–5 μM) compared with control (P5–P6 rats; $n = 6$). These results suggest that 5-HT_{2B}R and/or 5-HT_{2C}R exert a depolarizing action on E_{IPSP}. ns, $P > 0.05$; $*P < 0.05$; $**P < 0.01$ (Wilcoxon paired test).

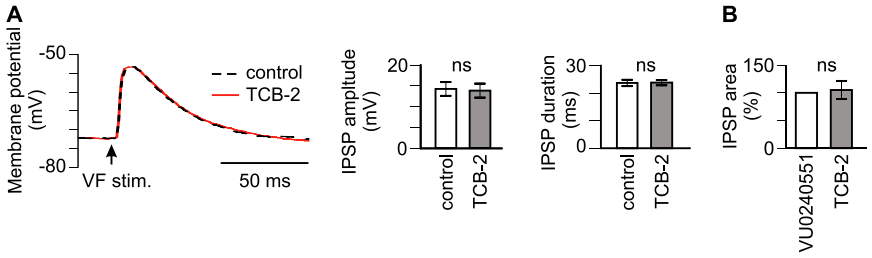

Fig. S3. TCB-2 has no effect on IPSP kinetics. (*A*) IPSP recorded by means of a microelectrode filled with KCl (2 M) to load the cell with Cl^- and, thereby, shift E_{IPSP}. The IPSP was quite similar before and after adding TCB-2 (0.1 μM). No significant difference was observed on both the amplitude (n = 6) (*Center*) and the duration (n = 6) (*Right*) of IPSPs from newborn rats (P4–P5). (*B*) The area of IPSPs was measured at V_{rest} before and after adding TCB-2 in the continuous presence of VU0240551 at 25 μM (P5–P6 rats; n = 11). ns, $P > 0.05$ (Wilcoxon paired test).

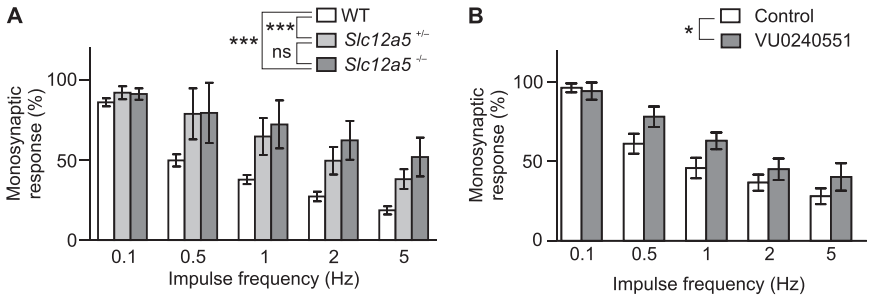

Fig. S4. RDD of the monosynaptic reflex in vitro is reduced when KCC2 function is genetically or pharmacologically reduced. (*A*) To investigate the role of KCC2 in this property of spinal cord reflexes, we used *Slc12a5*$^{+/-}$ mice (n = 7) and *Slc12a5*$^{-/-}$ mice (1) (n = 4), which retain ∼50% and 10% of normal KCC2 protein amounts in the spinal cord, respectively (2). RDD was significantly smaller in both types of mice compared with wild-type mice (n = 9), confirming that KCC2 cotransporters play a key role in the depression of the response. (*B*) The specific blockage of KCC2 by VU0240551 (25 μM; P5–P6 rats; n = 4) significantly decreases the RDD of the monosynaptic reflex. ns, $P > 0.05$; *$P < 0.05$; ***$P < 0.001$ (one-phase exponential decay regression).

1. Stil A, et al. (2011) Contribution of the potassium-chloride co-transporter KCC2 to the modulation of lumbar spinal networks in mice. *Eur J Neurosci* 33(7):1212–1222.
2. Woo NS, et al. (2002) Hyperexcitability and epilepsy associated with disruption of the mouse neuronal-specific K-Cl cotransporter gene. *Hippocampus* 12(2):258–268.

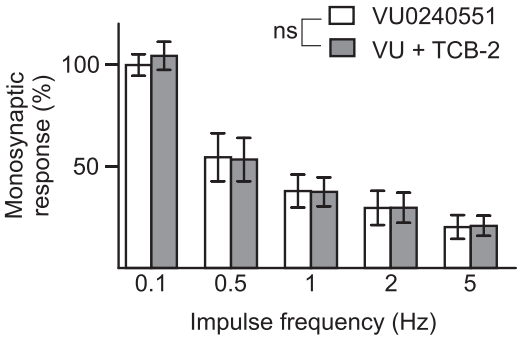

Fig. S5. Blocking KCC2 prevents the effect of TCB-2 on the RDD of the monosynaptic reflex in vitro. TCB-2 (0.1 μM) did not increase the RDD of the monosynaptic response in the continuous presence of the specific blocker of KCC2 (VU0240551; 25 μM; P5–P6 rats; n = 4). ns, $P > 0.05$ (Wilcoxon paired test).

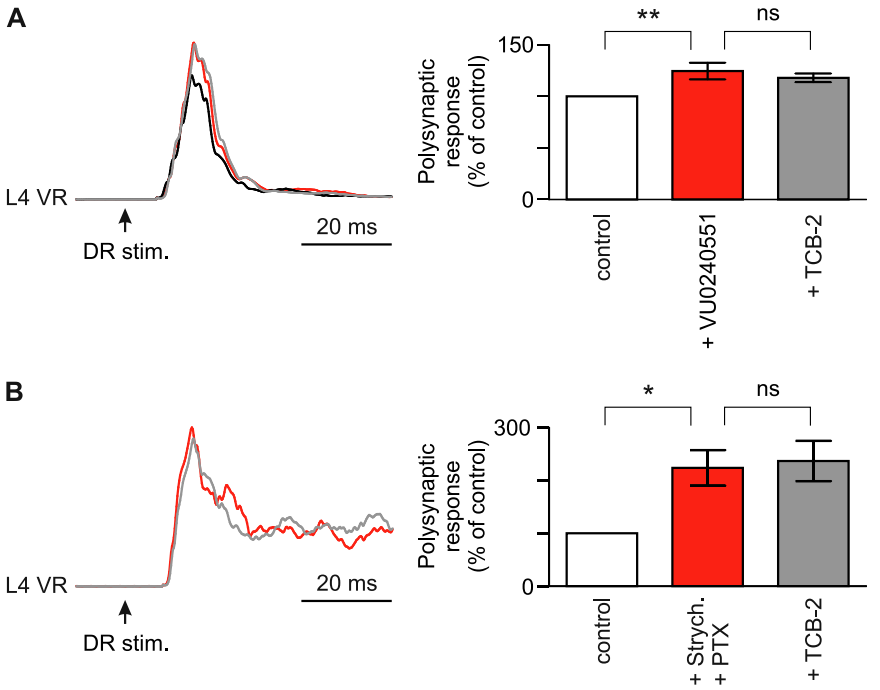

Fig. S6. TCB-2 reduces polysynaptic ventral root responses through a modulation of chloride homeostasis. (*A*) The specific blocker of KCC2 (VU0240551; 25 μM) significantly increased the polysynaptic ventral root responses and prevented the effect of TCB-2 on the polysynaptic response (P5 rats). ns, $P > 0.05$; $^{**}P < 0.01$ (Kruskal–Wallis test with Dunn's post test; $n = 4$ in each group). (*B*) The polysynaptic ventral root responses (rectified averaged signals) was significantly increased in presence of the GlyR and GABA receptor antagonists [strychnine and picrotoxin (PTX), respectively] compared with control conditions (P5–P6 rats). The decrease of the polysynaptic response by TCB-2 (0.1 μM) (Fig. 4) was prevented in the continuous presence of strychnine and PTX. ns, $P > 0.05$; $^{*}P < 0.05$ (Kruskal–Wallis test with Dunn's post test; $n = 4$ in each group).

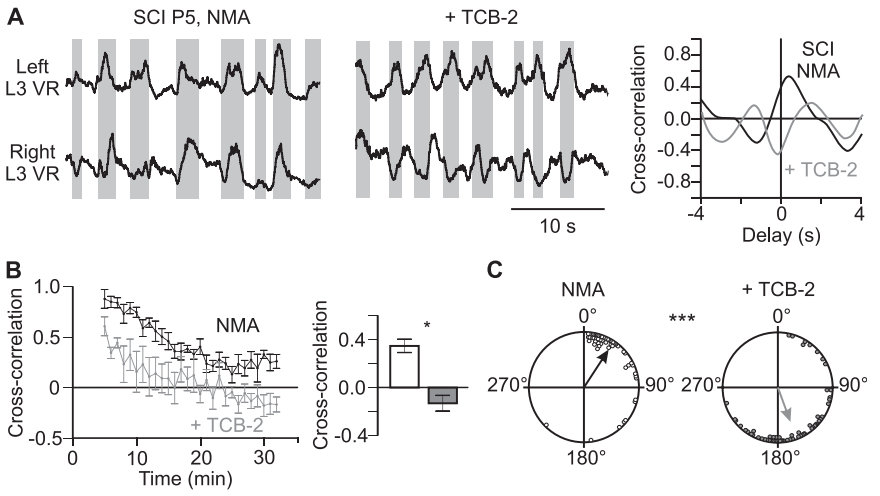

Fig. S7. Activation of 5-HT_{2A}Rs in vitro restores the left–right alternating locomotor pattern after neonatal spinal cord transection. (*A*) Integrated recordings from the left and right L3 ventral roots (VR) at P5 in the presence of NMA alone (16 μM) (*Left*) or together with 5-HT_{2A}R agonist TCB-2 (0.1 μM) (*Center*). Gray areas indicate the bursts occurring in the left L3 VR. Cross-correlograms between the two VR signals computed from 10 min of activity induced by NMA alone (black line) or NMA and TCB-2 (gray line). (*B*) Time course of the changes of cross-correlation coefficient in six transected rats in NMA alone (10–16 μM, black plot) or NMA and TCB-2 (0.1 μM, gray plot). Mean cross-correlation coefficient (*Right*) between left and right ventral root activities computed when activities were stable in both conditions (5–10 min). $^{*}P < 0.05$ (Wilcoxon paired test; $n = 6$). (*C*) Distribution of phase relationships between left and right ventral root bursts in NMA alone (*Left*) and NMA plus TCB-2 (*Right*) in all of the spinal animals (P5–P6; $n = 6$).

Table S1. Agonists/antagonists of 5-HT_2R and their receptor-binding affinity

		K_i (nM)		
Agonists [ref(s).]	Antagonists [ref(s).]	5-HT_{2A}R	5-HT_{2B}R	5-HT_{2C}R
DOI (1–3)		0.7	27.54	9.3
TCB-2 (4)		0.73	None	None
α-Methyl 5-HT (2, 3, 5)		127.05	10.47	2.69
	Ketanserin (3, 6)	1.49	740	59
	MDL11,939 (3)	26.3	3310	263.06
	SB206553 (3, 7)	2,300	5.5	3.2

1. Egan C, et al. (2000) Agonist high and low affinity state ratios predict drug intrinsic activity and a revised ternary complex mechanism at serotonin 5-HT(2A) and 5-HT(2C) receptors. *Synapse* 35(2):144–150.
2. Boess FG, Martin IL (1994) Molecular biology of 5-HT receptors. *Neuropharmacology* 33(3-4):275–317.
3. Knight AR, et al. (2004) Pharmacological characterisation of the agonist radioligand binding site of 5-HT(2A), 5-HT(2B) and 5-HT(2C) receptors. *Naunyn Schmiedebergs Arch Pharmacol* 370(2):114–123.
4. McLean TH, et al. (2006) 1-Aminomethylbenzocycloalkanes: Conformationally restricted hallucinogenic phenethylamine analogues as functionally selective 5-HT2A receptor agonists. *J Med Chem* 49(19):5794–5803.
5. Engel G, Göthert M, Hoyer D, Schlicker E, Hillenbrand K (1986) Identity of inhibitory presynaptic 5-hydroxytryptamine (5-HT) autoreceptors in the rat brain cortex with 5-HT1B binding sites. *Naunyn Schmiedebergs Arch Pharmacol* 332(1):1–7.
6. Aloyo VJ, Harvey JA (2000) Antagonist binding at 5-HT(2A) and 5-HT(2C) receptors in the rabbit: High correlation with the profile for the human receptors. *Eur J Pharmacol* 406(2): 163–169.
7. Cussac D, et al. (2002) Characterization of phospholipase C activity at h5-HT2C compared with h5-HT2B receptors: Influence of novel ligands upon membrane-bound levels of [3H] phosphatidylinositols. *Naunyn Schmiedebergs Arch Pharmacol* 365(3):242–252.

Table S2. Characteristics of the M and H waves before and 7 min after injection of TCB-2

	Before TCB-2 (mean ± SEM)	After TCB-2 (mean ± SEM)	Wilcoxon paired test (*P*)*
Threshold (mA)	2.35 ± 0.86	2.85 ± 1.09	0.25
M_{max} (mV)	3.42 ± 0.61	2.83 ± 0 0.33	0.13
I-M_{max} (mA)	4.10 ± 1.21	4.25 ± 1.40	0.75
H_{max} (mV)	1.90 ± 0.46	0.84 ± 0.14	0.13
I-H_{max}	3.26 ± 1.22	4.30 ± 1.39	0.20
H_{max}/M_{max}	0.55 ± 0.09	0.32 ± 0.09	0.13

The TCB-2 injection was 0.3 mg/kg, i.p.

*None of the paired comparison was significant ($P > 0.05$; $n = 4$).